Molecular Crystals and Liquid Crystals

ISSN: 1542-1406 (Print) 1563-5287 (Online) Journal homepage: http://www.tandfonline.com/loi/gmcl20

Phase Diagram Study of Succinonitrile-Vanillin Organic Alloy System

Jayram Singh, Preeti Gupta, S. S. Das & N. B. Singh

To cite this article: Jayram Singh, Preeti Gupta, S. S. Das & N. B. Singh (2014) Phase Diagram Study of Succinonitrile-Vanillin Organic Alloy System, Molecular Crystals and Liquid Crystals, 605:1, 240-258, DOI: 10.1080/15421406.2014.905034

To link to this article: http://dx.doi.org/10.1080/15421406.2014.905034

Published online: 15 Dec 2014.

Mol. Cryst. Liq. Cryst., Vol. 605: pp. 240–258, 2014

ISSN: 1542-1406 print/1563-5287 online
DOI: 10.1080/15421406.2014.905034

Taylor & Francis
Taylor & Francis Group

Phase Diagram Study of Succinonitrile-Vanillin Organic Alloy System

JAYRAM SINGH,[1] PREETI GUPTA,[2] S. S. DAS,[3] AND N. B. SINGH[1,*]

[1]Research and Technology Development Centre, Sharda University, Greater Noida, India
[2]Department of Materials Engineering, Indian Institute of Science, Bangalore, India
[3]Department of Chemistry, DDU Gorakhpur University, Gorakhpur, India

Phase diagram studies of succinonitrile-vanillin system show the formation of 2:1 congruent melting type compound. Crystallization velocities of pure components, succinonitrile-vanillin complex, and two eutectics have been determined at different undercoolings. On the basis of heat of fusion measurements, excess thermodynamic functions have been calculated. Microstructural studies revealed that impurities modify the morphology. FTIR spectral studies and computer simulation have shown the existence of hydrogen bonding in the eutectics and the congruent melting compound. On the basis of experimental results, the mechanism of formation of eutectics and its solidification behavior are discussed.

Keywords: Enthalpy of fusion; entropy of fusion; eutectic; excess functions; phase equilibria

1. Introduction

Organic eutectic systems have widely been used as a model system for predicting various properties of metallic alloys. Modern technology demands low cost, superior quality, and high-strength materials. In recent years [1–8], it is found that composite materials exhibit such properties. One of the important methods of preparing such composite materials is through unidirectional solidification so that the required microstructure is obtained. Further crystallization technology for the separation and purification of organic materials is also used widely because of the low energy consumption and higher purity. So the study of solid–liquid equilibria is of interest for the development of theoretical models and their application in the chemical industry. During the last few years, the phase diagram, solidification behavior, microstructures, and other properties of binary organic systems forming eutectic mixtures and congruent melting compounds (CMC) have been studied [9–16]. However, different systems under different conditions exhibit different properties. Therefore, it is essential to study large number of such systems so that the

*Address correspondence to N. B. Singh. Research and Technology Development Centre, Sharda University, Greater Noida, India. E-mail: nbsingh43@gmail.com

Color versions of one or more of the figures in the article can be found online at www.tandfonline.com/gmcl.

desired materials can be prepared and their properties predicted. In this paper, phase diagram of succinonitrile (SCN)-vanillin (VN) system has been investigated and the results discussed.

2. Experimental

2.1. Materials

SCN (*Alfa Aesar*) was used without further purification (melting temperature 330.2 K). VN (*SDDFCL*) was purified by repeated crystallization from hot water (melting temperature 354.2 K). The structures of SCN and vanillin are given in Fig. 1.

2.2. Methods

2.2.1. Phase Diagram Studies. The phase diagram of SCN-VN system was studied by the thaw melt method [17]. Mixtures of different compositions of SCN and VN were prepared by melt and quenching method, homogenized, and determined their thaw and melting temperatures with the help of a precision thermometer which could read up to (0.1 K). The thaw points and melting points of different mixtures are given in Table 1. These melting points were plotted against composition to construct the phase diagram (Fig. 2).

2.2.2 Undercooling Measurements. Undercooling measurements were made as described earlier [17]. Different compositions of SCN-VN mixture were taken in clean glass tubes. The glass tubes were sealed and immersed in liquid paraffin oil bath maintained at a temperature slightly above their melting temperatures to destroy any germ nuclei. After complete melting of the material, the temperature of the bath was allowed to cool at constant rate. The formation of first crystallite was noticed by a magnifying glass and each experiment was repeated at least five times. The temperature at which the first crystallite appeared was noted. The difference between the true melting temperature and this temperature gave the undercooling temperature. The undercooling values of different mixture of SCN-VN system were recorded and are given in Table 1.

2.2.3. Linear Velocity of Solidification. Linear velocities of crystallization were determined by the method as described earlier [18]. U-shaped Pyrex glass tubes of length 11 cm

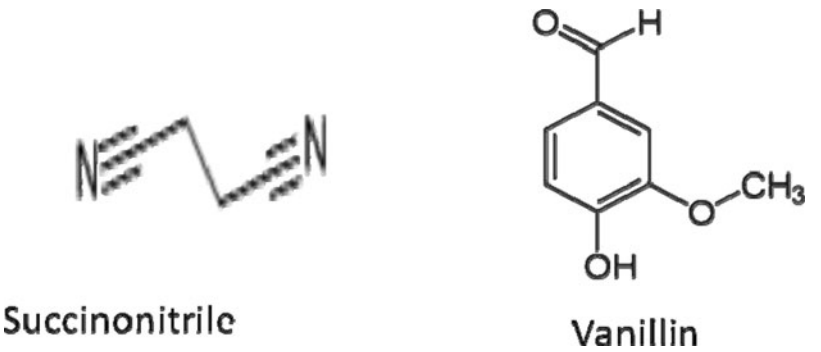

Figure 1. Structures for pure components SCN and VN.

Table 1. Temperature-composition data for SCN-VN system

X_{SCN}	Solidus Temperature (T_S) (K)	Liquidus temperature (T_L) (K)	Temperature at first nuclei appear (T) (K)	$\Delta T = T_L - T$ ($K \pm 0.0$)
0.0000	—	354.8 ± 0.0	348.4 ± 0.0	6.4
0.1644	321.3 ± 0.0	356.8 ± 0.0	348.4 ± 0.0	8.4
0.3165	321.2 ± 0.0	353.8 ± 0.0	344.3 ± 0.0	9.5
0.4419	321.3 ± 0.0	347.5 ± 0.0	337.7 ± 0.0	9.8
0.5568	321.8 ± 0.0	338.3 ± 0.0	330.3 ± 0.0	8
0.6087	321.4 ± 0.0	334.4 ± 0.0	324.7 ± 0.0	9.7
0.6495[a]	—	321.6 ± 0.0	317.4 ± 0.0	4.2
0.6771	321.2 ± 0.0	328.3 ± 0.0	323.8 ± 0.0	4.5
0.7041	321.5 ± 0.0	331.4 ± 0.0	325.9 ± 0.0	5.5
0.7500[b]	—	333.6 ± 0.0	328.9 ± 0.0	4.7
0.8182	311.4 ± 0.0	330.5 ± 0.0	325.6 ± 0.0	4.9
0.8783	311.9 ± 0.0	325.3 ± 0.0	319.7 ± 0.0	5.6
0.9426	311.4 ± 0.2	318.3 ± 0.0	313.3 ± 0.0	5
0.9756[c]	—	311.9 ± 0.0	308.1 ± 0.0	3.8
0.9919	311.4 ± 0.0	319.4 ± 0.0	313.9 ± 0.0	5.5
1.0000	—	330.2 ± 0.0	327.2 ± 0.0	3

[a]Eutectic E_1.
[b]eutectic E_2.
[c]CMC.

and diameter 0.5 cm were filled with a solid material and kept in an oil thermostat at a temperature slightly above their melting temperatures. A seed crystal was introduced from one side of the tube, where crystallization started and the measurements were made at different undercooling. Time required for crystallization for a definite length of the tube in the horizontal part was recorded.

2.2.4. Microstructural Studies. Small amount of fine powders of SCN, VN, CMC, and eutectic mixtures E_1 and E_2 were placed on separate glass slides and kept in an oven at a temperature slightly above their melting temperatures. The melts were crystallized by moving separate glass cover slips gently pressed over them in one direction. The microphotographs of the crystallized fronts were recorded with the help of digital camera attached to an optical microscope (Olympus Chi20). The microstructures were also recorded in the presence of different impurities also.

2.2.5. Mechanical Strength. In order to determine the mechanical strengths, the samples were melted in a uniform cylindrical glass tube and then dropped vertically into ice bath maintained at $\sim 0^{\circ}$C in order to have samples in cylindrical form [14]. These cylindrical samples, removed from the tubes, were placed on the stand. A small container was hung in the middle of the cylindrical sample with the help of a metallic wire. The modulus of rupture (σ_{fs}) of the materials was calculated using Eq. (1) [19];

$$\sigma_{fs} = \frac{F_f\, L}{\pi\, R^3} \tag{1}$$

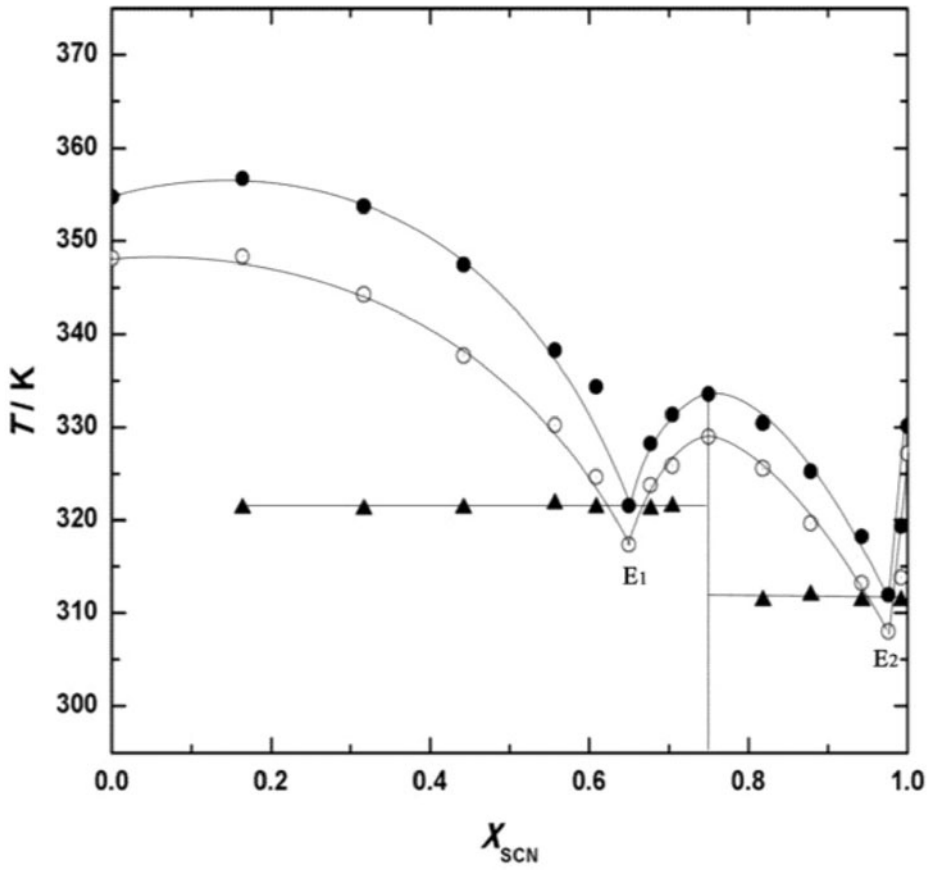

Figure 2. Temperature-composition diagram for SCN-VN congruent melting system: ▲, solidus temperature; ●, liquidus temperature; ○, undercooling.

where F_f is the load at fracture; L is the distance between support points; and R is the specimen radius.

2.2.6. Differential Thermal Analysis. Differential thermal analysis (DTA) of pure components, CMC, and eutectic mixtures E_1 and E_2 were performed using TG-DTA instrument, NETZSCH STA 409. Powders of samples were taken in alumina crucible with alumina lid and a blank crucible was taken as a reference. The analysis was carried out in nitrogen atmosphere from room temperature to 523 K at a heating rate of 5 K min^{-1}.

2.2.7. FTIR Spectral Studies. FTIR spectra of SCN, VN, CMC, E_1, and E_2 were recorded with a FTIR spectrophotometer in KBr phase.

2.2.8. Computational Studies. In order get ideas about the nature of interaction taking place between the two components undertaken during the present studies, interaction energy between the components was calculated using density functional theory. Gaussian 09 was used for all calculations. The basis set used during the present calculation was taken to be 6-31G(d). The optimization of the species are done at DFT (B3LYP)/(6-31G(d)) level of the

theory. The vibrational frequency calculations were also made at the optimized structures using the same level of the theory in order to see that the structures were at minima on their potential energy surface. Zero point corrected total energies of the species were taken into account for the calculation of the interaction energy. It is defined as:

$$\Delta E_{\text{interaction}} = E_{(\text{vn}-\text{scn})} - E_{\text{vn}} - E_{\text{scn}}. \tag{2}$$

where $\Delta E_{\text{interaction}}$ is the interaction energy between the VN and SCN and $E_{(\text{vn-scn})}$, E_{vn}, and E_{scn} are the zero-point corrected total energies of the complex and the two individual components.

In the calculation, the structures of VN, SCN, and CMC were first optimized and then frequency was calculated.

3. Results and Discussion

3.1. Phase Diagram

Temperature-composition diagram for the system SCN-VN has been studied by thaw melt method and represented in Fig. 2. The phase diagram curve revealed that SCN combines with VN in 2:1 molar ratio forming a CMC enclosed by two eutectics E_1 and E_2. CMC melts at 333.6 K. Vanillin-SCN phase diagram shows flat maxima which attributes that the CMC is stable in solid state and dissociates in molten state. The first eutectic mixture E_1 is formed at 0.6495 mole fraction of SCN which melts at 321.6 K. Eutectic mixture E_2 is formed at 0.9756 mole fraction of SCN with melting temperature 311.9 K. Undercooling temperatures for pure components and all, the compositions are also measured and represented in the same figure (Fig. 2). The undercooling curve is similar to the melting temperature curve. The solid–liquid equilibrium data are given in Table 1.

3.2. Crystallization Studies

Hillig-Turnbull [20] proposed an equation to relate the linear velocity of crystallization to its undercooling temperature:

$$v = k(\Delta T)^{\text{n}}$$

$$\log\, v = \log\, k + n\, \log \Delta T \tag{3}$$

where v denotes the linear velocity of crystallization, ΔT is the degree of undercooling (difference between the melting temperature and the temperature at which first crystallite appears), k is kinetic coefficient, and n is a constant.

Log v when plotted against log ΔT for pure SCN, pure VN, CMC, and eutectic E_1 and E_2 straight lines are obtained (Fig. 3) showing the validity of Hillig-Turnbull relationship (Eq. 3). Kinetic coefficient (k) and constant (n) are calculated from the intercepts and slopes of the straight lines respectively. The values of k and n for pure components, CMC and two eutectic mixtures are given in Table 2.

Assuming that eutectic is a mechanical mixture of the two components, the linear velocity of crystallization should obey the mixture law Eq. (4).

$$v_{\text{e}} = x_1 v_1 + x_2 v_2 \tag{4}$$

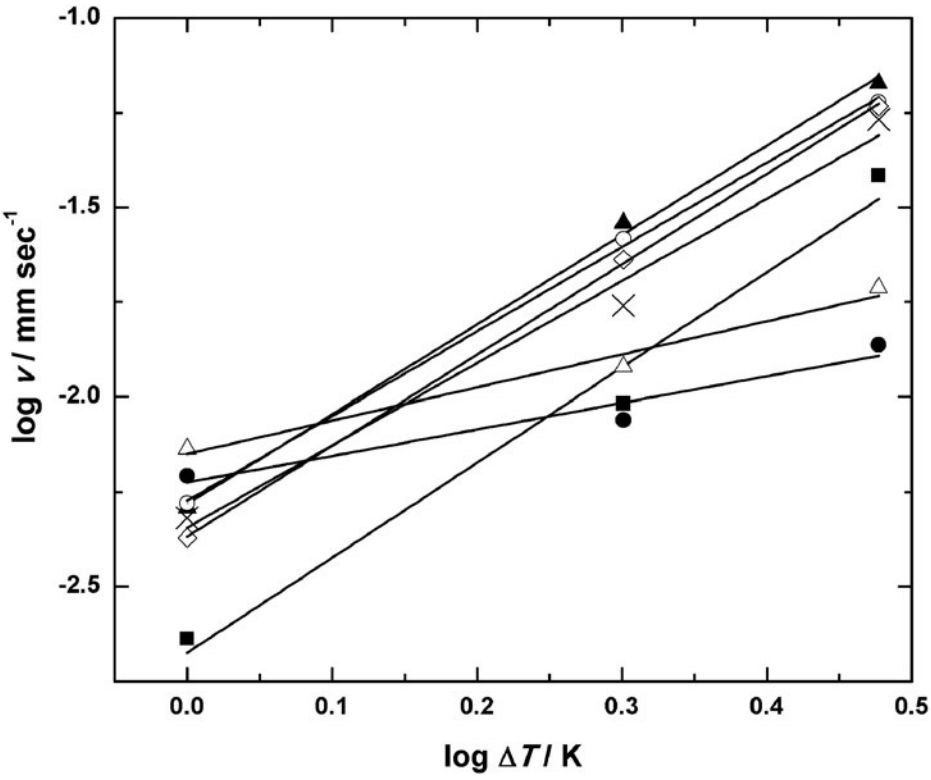

Figure 3. Verification of $v = k\,(\Delta T)^n$ in SCN–VN system; ■, SCN; ●, vanillin; ▲, CMC; △, eutectic E_1; ○, eutectic E_1 (mix law); ×, eutectic E_2; ◊, eutectic E_2 (mix law).

where x_1 and x_2 are the mole fractions, v_1 and v_2 are the linear velocities of crystallization of pure components 1 and 2, respectively. Linear velocity of crystallizations at different ΔT for two eutectic mixtures E_1 and E_2 calculated by using mixture law are also given in Fig. 3. Values of k and n computed for the eutectic mixtures E_1 and E_2 by employing mixture law is also given in Table 2. Figure 3 signifies that the linear velocity of crystallization for the two components, CMC, and E_1 and E_2 increase with increasing undercooling

Table 2. Values of linear velocity of crystallization of SCN-Vanillin congruent melting system at different undercooling (ΔT)

Components	k (mm s^{-1} K^{-1})	n
SCN	−2.22 (±0.1)	0.69 (±0.32)
Vanillin	−2.68 (±0.24)	2.51 (±0.72)
CMC	−2.28 (±0.04)	2.36 (±0.11)
Eutectic E_1	−2.15 (±0.08)	0.87 (±0.26)
Eutectic E_1 (mixture law)	−2.27 (±0.02)	2.23 (±0.07)
Eutectic E_2	−2.34 (±0.16)	−2.16 (±0.50)
Eutectic E_2 (mixture law)	−2.37 (±0.11)	−2.39 (±0.35)

(ΔT). Experimental values for linear velocity of crystallization of the eutectic mixtures are different from those calculated by mixture law (Eq. 3). This indicates the presence of some weak interaction in the eutectic mixtures.

Solidification of eutectics can be predicted on the basis of Winegard theory [21]. According to this theory, the formation of nucleus is the initialization of the eutectic solidification. This phase would grow until the surrounding liquid become richer in the other component and reaches at a stage when the second component starts nucleating. There are two possibilities of nucleation; side by side growth of the two components and alternate nucleation of the two initial crystals. In the side by side growth, the rate of crystallization of eutectic materials is lower than that of the pure components. However in alternate growth, the linear velocity of crystallization of eutectic mixtures is higher than that of any one of the two pure components. Eutectic E_1, which is formed between vanillin and CMC, has higher value of linear velocity of crystallization than vanillin and CMC. This implies that eutectic E_1 may possess alternate growth. Linear velocity of crystallization of Eutectic E_2 (formed between CMC and SCN) is lower than CMC and Higher than SCN. This suggests that side by side growth can occur in E_2.

3.3. Thermodynamic Properties

Using differential thermal analysis, enthalpy of fusion of the pure components, CMC, eutectic E_1, and eutectic E_2 are measured. The values of the enthalpies of fusion are presented in Table 3. If a solid eutectic mixture behaves ideally then its enthalpy of fusion can be calculated using mixture law, Eq (5):

$$(\Delta_{\mathrm{f}} H)_{\mathrm{e,mix\,law}} = (x_1)_{\mathrm{e}}(\Delta_f H)_1 + (x_2)_{\mathrm{e}}(\Delta_{\mathrm{f}} H)_2 \tag{5}$$

where $(x_1)_{\mathrm{e}}$ and $(x_2)_{\mathrm{e}}$ are the mole fractions of the two components in the eutectic mixture and $(\Delta_{\mathrm{f}}H)_1$ and $(\Delta_{\mathrm{f}}H)_2$ are the enthalpies of fusion of the pure component 1 and 2, respectively.

In the process of melting of eutectic mixtures, some sort of mixing and association may take place [22, 23]. The enthalpy of fusion of eutectic mixture is related with enthalpy of mixing ($H_{\mathrm{m}}{}^{\mathrm{l}}$), solid-liquid interfacial energy ($\sigma_{\mathrm{LS}}\mathrm{A}$), and a constant ε, as given by Eq. (6).

$$(\Delta H_{\mathrm{f}})_{\mathrm{e}} = [(\Delta H_{\mathrm{f}})_{\mathrm{e}}]_{\mathrm{mix.law}} + H_m^l + \sigma_{\mathrm{LS}} A + \varepsilon \tag{6}$$

where $H_m^l + \sigma_{\mathrm{LS}} A + \varepsilon$ is the total interaction energy which arises due to non-ideal nature of the eutectic mixture. The total interaction energy $\left(H_m^l + \sigma_{\mathrm{LS}} A + \varepsilon\right)$ for each system is calculated using Eq. (6).

Enthalpy of fusions for both the eutectics, E_1 and E_2, are calculated from Eq. 5 and are given in Table 3. The interaction energies for eutectic mixtures are also calculated employing Eq. 6 and are given in the same table (Table 3). The nonideal nature of the two eutectics in the molten state can be predicted with the help of their heat of fusion values and excess thermodynamic functions. The heat of fusion is the property of a particular phase, which will be influenced in the presence of another phase. The eutectic mixture consists of two solid phases and its heat of fusion value will depend on the nature of interaction between the two types of molecules in the molten state. Heats of fusion values of the components and the eutectic mixtures as determined from DTA and calculated by using the mixture law Eq. 5 are given in Table 3. The values suggest that the experimentally determined heat of fusion value of eutectic mixtures is lower than the calculated values.

Table 3. Values of enthalpy of fusion ($\Delta_f H$), entropy of fusion ($\Delta_f S$), interaction energy, and Jackson's Roughness parameter (α) for SCN-VN congruent melting systems

Component	$\Delta_f H$ (experimental) kJ mol^{-1}	$\Delta_f H$ (calculated by mixture law) kJ mol^{-1}	Interaction energy kJ mol^{-1}	$\Delta_f S$ J mol^{-1} K^{-1}	Jackson's Roughness parameter (α)	
					$\xi = 0.5$	$\xi = 1.0$
SCN	0.82	—		2.48	0.15	0.29
VN	7.79	—		21.96	1.32	2.64
CMC	7.03	—		21.08	1.27	2.5
Eutectic E_1	1.62	7.13	−5.51	5.02	0.3	0.6
Eutectic E_2	2.81	5.16	−2.35	9.02	0.54	1.08

This indicates that some weak interactions may exist between the two components in the eutectic mixtures.

Concept of excess thermodynamic functions plays a key role to understand the interaction between the components of a mixture. Excess Gibbs energy (G^E), excess entropy (S^E), and excess enthalpy (H^E) were calculated in a similar way as reported earlier [12–16]. The phase diagram of SCN-VN is divided into two parts, so as to make two simple eutectic type systems VN-CMC and CMC-SCN. Excess thermodynamic functions, i.e., G^E, S^E, and H^E for SCN-VN system is represented in Tables 4(a) and 4(b) and plotted as function of mole fraction of X_{CMC} in Figs. 4(a) and 4(b). In vanillin-CMC system, the values of H^E is negative and minimum at eutectic composition E_1. After eutectic composition the values become positive. S^E values are negative for the preeutectic mixture and positive for posteutectic mixtures. Values for G^E for whole composition are positive and decrease with increasing value of X_{CMC}. Considering the values of G^E, it can be stated that the stability of posteutectic mixtures are higher than that of preeutectic mixtures. It is seen that in the CMC-SCN eutectic system, the values for S^E and H^E for entire composition range are negative with increasing trend. On the contrary, G^E values are positive and minimum at $X_{CMC} = 0.0909$.

Results of excess functions reveal that the pre- and posteutectic mixtures in both the simple eutectic systems, VN-CMC and CMC-SCN, possess positive deviation from ideal behavior.

3.4. Microstructural Studies

Microstructures of SCN, VN, CMC, and eutectics E_1 and E_2 in the absence and presence of impurities are shown in Fig. 5. Microstructure of SCN (Fig. 5 (a)) shows fractal type structure whereas the microstructure of VN (Fig. 5 (b)) indicates that the crystallization starts from a central point. Microstructures of Eutectics E_1 and E_2 are shown in Figs. 5(c) and 5(d), respectively and both have distorted lamellar structures. In the presence of β-naphthol as an impurity in E_1 (Fig. 5(e)), structural regularity is lost whereas 8-hydroxyquinoline changed the microstructure into rod shaped oriented in different directions (Fig. 5(f)). Microstructure of E_2 in the presence of impurities is changed completely and rectangular shaped crystals oriented in different directions are obtained (Figs. 5(g) and 5(h)). The microstructure of CMC (Fig. 5(i)) shows interlocking type structure arranged in strips which changed drastically in the presence of impurities (Figs. 5(j) and 5(k)). Thus the impurities change the microstructures. It is already reported that when roughness factor, α, is greater than 2, the solid–liquid interface is atomically smooth and the crystal develops a faceted morphology and whenthe value is less than 2, nonfaceted morphology is developed (Table 3) [24, 25]. It appears that the type of interaction in the system affects the formation of critical nuclei which in turn determines the microstructure. Impurities modify the interactions and hence change the microstructures.

3.5. FTIR Spectral Studies

FTIR spectra (Fig. 6) show that there is a strong hydrogen bonding in vanillin molecule (3176 cm^{-1}). However when eutectics and CMC are formed, the hydrogen bond with in vanillin molecule is broken and a new hydrogen bond with N atom of SCN and H atom of OH group of VN is formed (3400 cm^{-1}). The presence of hydrogen bonding is responsible for the stability and definite geometry.

Table 4a. Excess Gibbs energy (G^E), excess entropy (S^E), and excess enthalpy (H^E) for VN-CMC in SCN-VN congruent melting system

X_{SCN}	T_m (K)	X_{CMC}	X_{VN}	ln γ_{CMC}	ln γ_{VN}	$\frac{\partial \ln \gamma_{CMC}}{\partial T}$	$\frac{\partial \ln \gamma_{VN}}{\partial T}$	G^E (kJ mol^{-1})	S^E (J K^{-1}mol^{-1})	H^E (kJ mol^{-1})
0.1644	356.6	0.2192	0.7808	1.4234	−0.0267	0.0876	−0.015	0.8668	−24.61	−7.9134
0.3165	353.6	0.422	0.578	0.7684	0.2738	0.0491	−0.0229	1.4216	−26.1	−7.8116
0.4419	347.3	0.5892	0.4108	0.4346	0.6153	0.0374	−0.0352	1.4714	−26	−7.5602
0.5568	338.1	0.7424	0.2576	0.2035	1.0819	0.0312	−0.0606	1.2095	−24.83	−7.1862
0.6087	334.2	0.8116	0.1884	0.1144	1.3948	0.0292	−0.0856	0.9891	−23.99	−7.0308
0.6495	321.4	0.866	0.134	0.0495	1.7355	0.0278	−0.1234	0.7367	−22.54	−6.5093
0.6771	328.1	0.9028	0.0972	0.0079	2.0566	−0.0174	0.0645	0.5652	23.97	8.4282
0.7041	331.2	0.9388	0.0612	−0.0312	2.5192	−0.0169	0.1078	0.3442	24.48	8.4533

Table 4b. Excess Gibbs energy (G^E), excess entropy (S^E), and excess enthalpy (H^E) for CMC-SCN in SCN-VN congruent melting system

X_{SCN}	T_m (K)	X_{CMC}	X_{SCN}	ln γ_{CMC}	ln γ_{SCN}	$\frac{\partial \ln\gamma_{CMC}}{\partial T}$	$\frac{\partial \ln\gamma_{SCN}}{\partial T}$	G^E (kJ mol^{-1})	S^E (J K^{-1} mol^{-1})	H^E (kJ mol^{-1})
0.8182	330.3	0.0909	0.9091	−0.0801	2.3804	−0.0062	0.0675	0.3944	−20.01	−5.6692
0.8783	325.1	0.1711	0.8289	0.0122	1.7485	−0.0077	0.0453	0.8357	−19.16	−4.9441
0.9426	318.1	0.2568	0.7432	0.1213	1.3422	−0.0087	0.0388	1.1501	−18.49	−4.5118
0.9756	311.8	0.3008	0.6992	0.1824	1.1841	0.0118	−0.0097	1.2538	−17.75	−4.2796
0.9919	319.2	0.3225	0.6775	0.2139	1.1143	0.0119	−0.0091	1.3384	−17.81	−4.3456

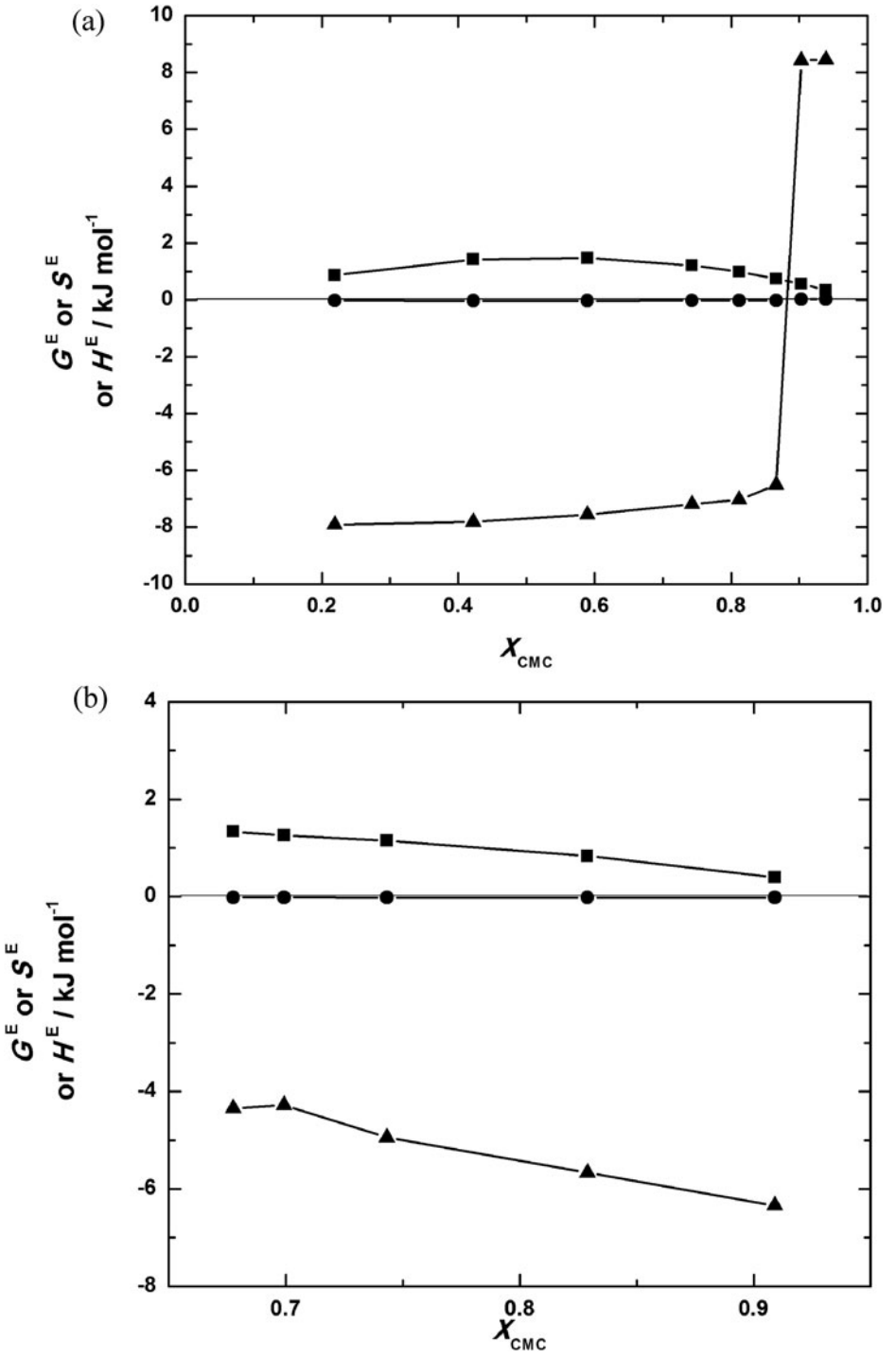

Figure 4. (a) G^E, H^E, and S^E values of CMC-VN in SCN-VN congruent melting system: ■, G^E; ●, S^E; ▲, and H^E. (b) G^E, H^E, and S^E values of CMC-SCN in SCN-VN congruent melting system: ■, G^E; ●, S^E; ▲, and H^E.

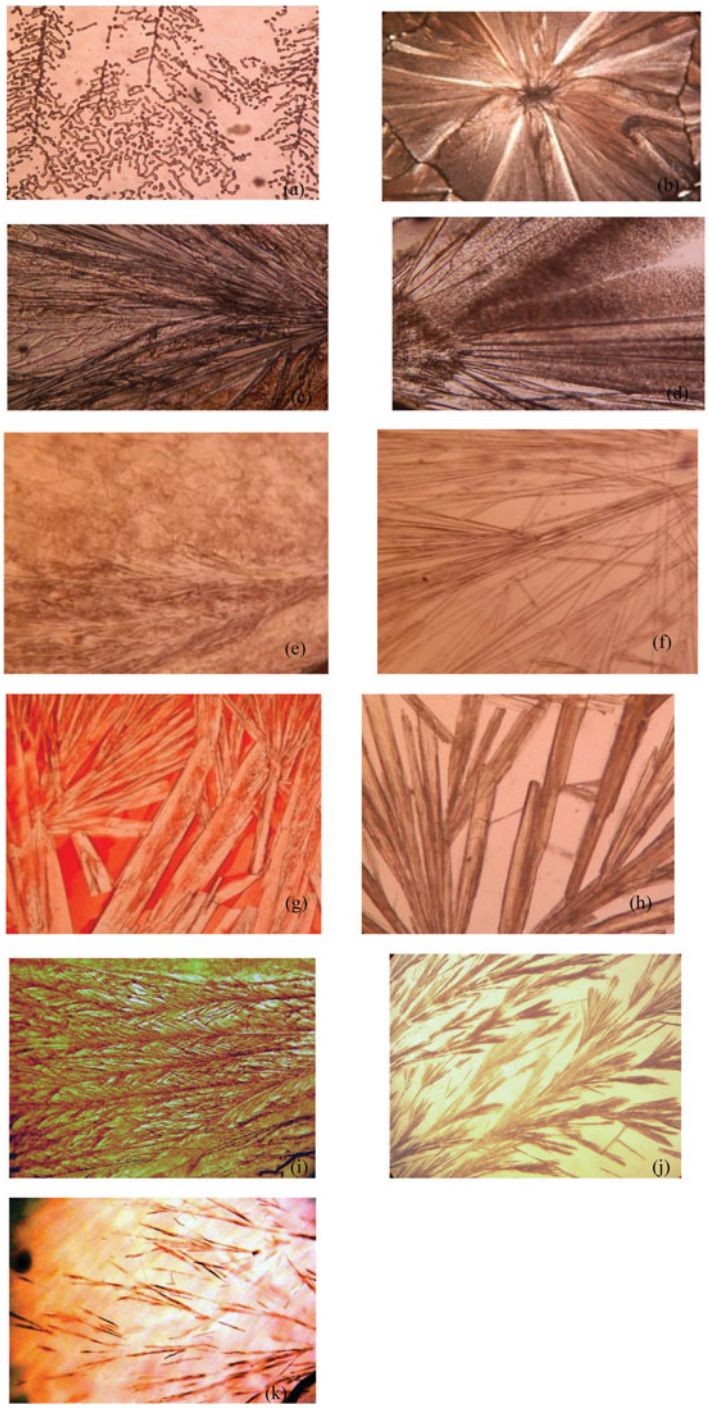

Figure 5. Microstructures: (a) SCN, (b) VN, (c) eutectic E_1, (d) eutectic E_2, (e) eutectic E_1 + β-naphthol, (f) eutectic E_1 + 8-hydroxyquinoline, (g) eutectic E_2 + β-naphthol, (h) eutectic E_2 + 8-hydroxyquinoline, (i) CMC, (j) CMC + β-naphthol, and (k) CMC + 8-hydroxyquinoline.

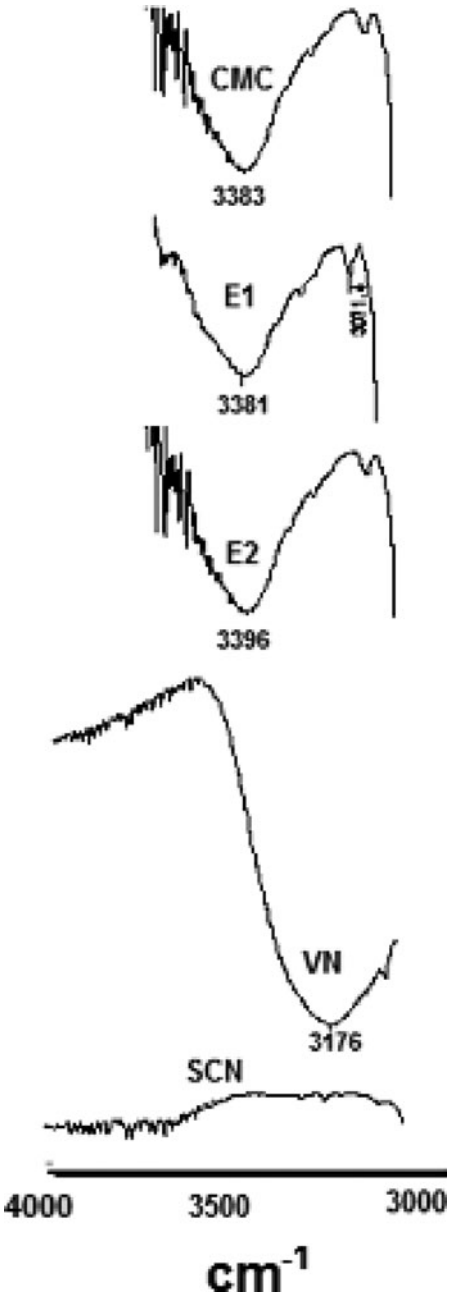

Figure 6. FTIR spectra for SCN, VN, eutectic E_1, eutectic E_2, and CMC.

3.6. Mechanical Strength

Values of modulus of rupture for the components, CMC, and eutectics are given in Table 5. The values for CMC and the eutectics are lower than that of pure components, which may be due to differences in nature of interaction and crystallizational behavior.

Table 5. Values of modulus of rupture of SCN-VN system

Components	Modulus of rupture (M Pa)
SCN	0.5344 ± 0.08
VN	1.3157 ± 0.05
CMC	0.4041 ± 0.01
Eutectic E_1	0.3689 ± 0.03
Eutectic E_2	0.3002 ± 0.06

3.7. Computer Simulation

The optimized geometries of SCN, VN, and CMC are given in Fig. 7 and the interaction energy is calculated in the following manner.

$$\begin{aligned}\Delta E\,(\text{Interaction in Hartree}) &= E(\text{CMC}) - E(\text{VN}) - E(\text{SCN}) \\ &= (-799.387057847) - (-534.923254812) \\ &\quad -(-264.218968221) = -0.244834814\,\text{Hartree} \qquad (7)\end{aligned}$$

Table 6. Computational values

Parameters	VN	SCN	CMC
Energy (Hartree)	−534.923254812 A.U. after 1 cycles	−264.218968221 A.U. after 1 cycles	−799.387057847 A.U. after 1 cycles
Zero-point vibrational energy (J mol^{-1})	368654.2	193988.2	583479.5
Zero-point vibrational energy (kcal mol^{-1})	88.11047	46.36429	139.45494
Zero-point correction (Hartree/Particle)	0.140413	0.073886	0.222236
Thermal correction to energy	0.149527	0.080064	0.240510
Thermal correction to enthalpy	0.150472	0.081008	0.241455
Thermal correction to Gibbs energy	0.105645	0.044533	0.170283
Sum of electronic and zero-point energies	−534.782842	−264.145082	−799.164822
Sum of electronic and thermal energies	−534.773727	−264.138904	−799.146547
Sum of electronic and thermal enthalpies	−534.772783	−264.137960	−799.145603
Sum of electronic and thermal free energies	−534.817610	−264.174435	−799.216775

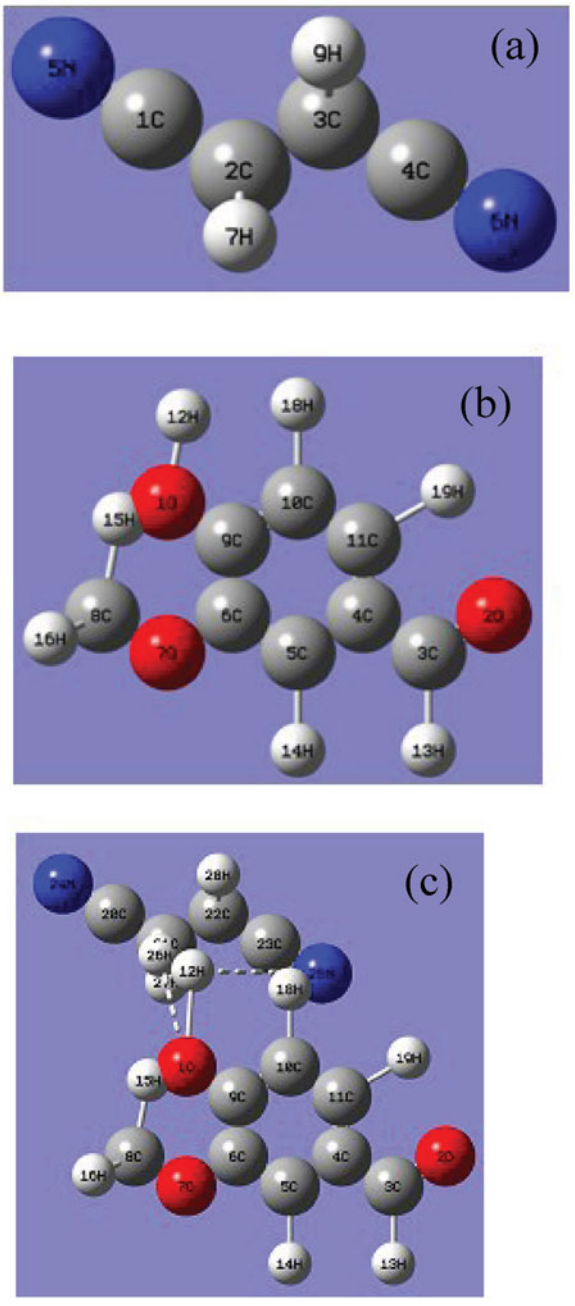

Figure 7. Optimized geometries: (a) SCN, (b) VN, and (c) CMC.

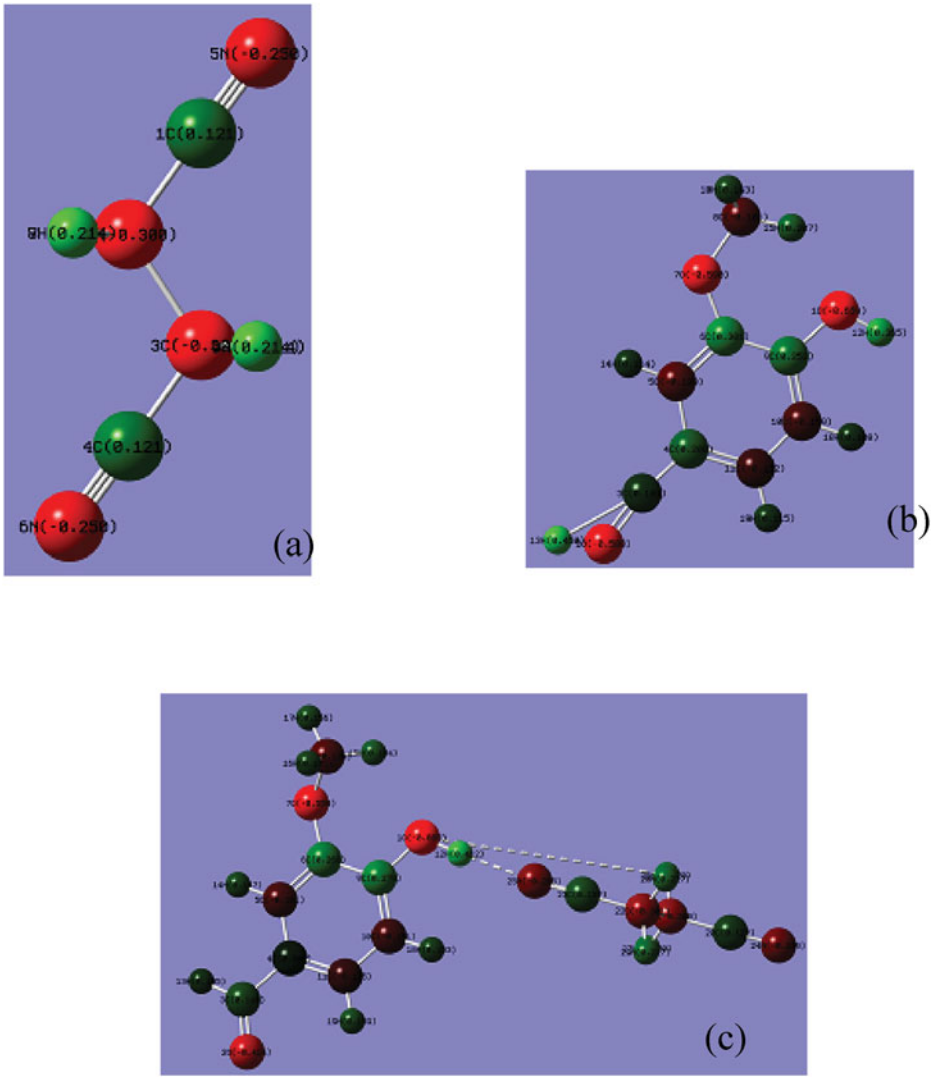

Figure 8. of Mulliken charges: (a) SCN, (b) VN, and (c) CMC

Representation of Mulliken charges on the three structures are given in Fig. 8. HUMO and LUMO of SCN, VN, and their mixture are given in Fig. 9. Different computational values are given in Table 6.

The computational studies performed at the DFT level show the formation of H-bonds between the two components via N—H and O—H. The optimized structures of the complex and the two species as given in Fig. 7 show that the structure of the complex does not vary significantly. The components are interacting together with interaction energy of 19.28 kJ mol^{-1} showing existence of the hydrogen bond type interaction. The distance of about 2.5 Å between N—H and O—H of the two components envisages that the hydrogen bonds are predominant in the formation of the complex between VN and SCN.

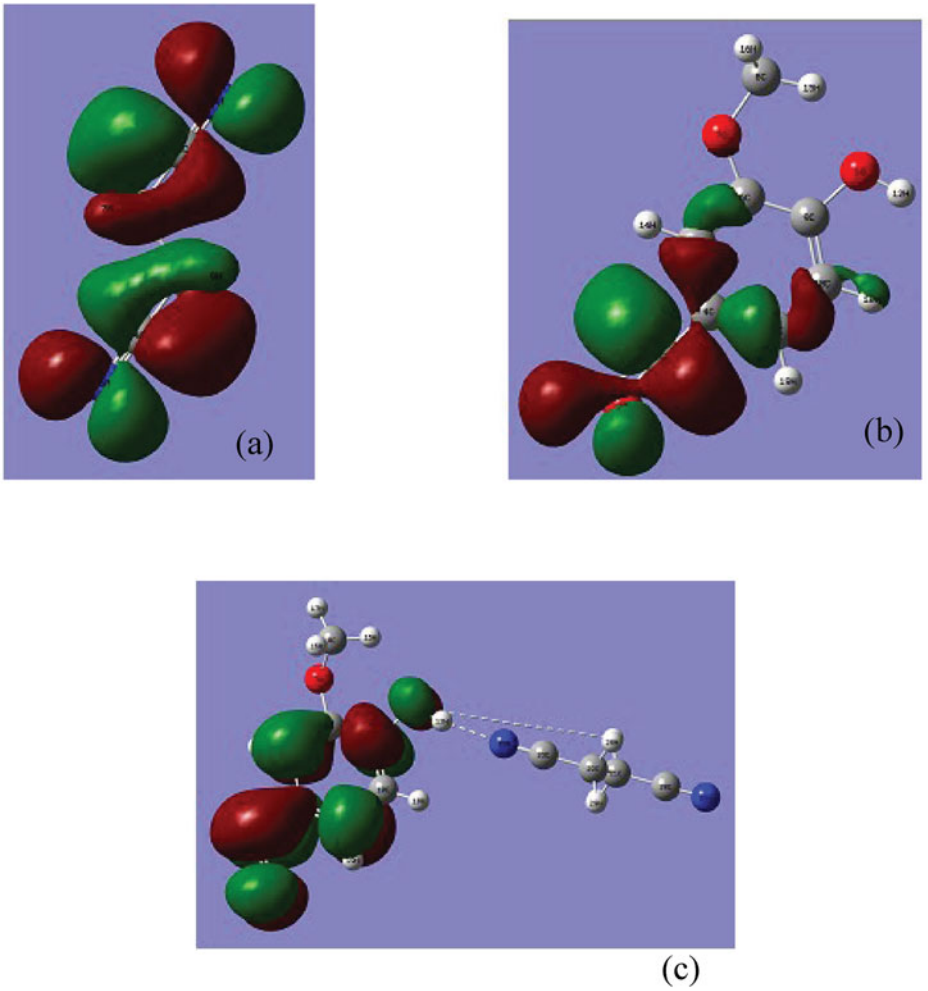

Figure 9. HUMO and LUMO: (a) SCN, (b) VN, and (c) CMC.

4. Conclusions

Phase diagram studies have shown that SCN-VN system form congruent melting type compound in 2:1 molar ratio. Linear velocities of crystallization, mechanical strength, undercooling measurements, and excess thermodynamic functions have shown non ideal behavior of eutectic mixtures. Microstructural investigations have indicated that the microstructures change from system to system and modified in the presence of impurities. FTIR spectral and computer simulation studies have shown the presence of H-bonding in the eutectics and the CMC.

References

[1] Witusiewicz, V. T., Hecht, U., Rex, S., & Apel, M. (2005). *Acta Mater.*, *53*, 3663.
[2] Cui, C., Zhang, J., Wu, G., Su, H., Han, M., Liu, L., & Fu, H. (2007). *J. Cryst. Growth*, *309*, 93.
[3] Sharma, B. L. (2004). *J. Alloys Compd.*, *385*, 74.

[4] Hassel, A. W., Bello, R. B., Milenkovic, S., & Scheider A. (2005). *Electrochim. Acta*, *51*, 795
[5] Sharma, B. L., Tandon, S., & Gupta, S. (2009). *Cryst. Res. Technol.*, *44*, 258.
[6] Asta, M. *et al.* (2009). *Acta Mater.*, *57*, 941.
[7] Gupta, R. K., & Singh, R. A. (2004). *J. Cryst. Growth*, *267*, 340.
[8] Singh, N. B., Das, S. S., Singh, N. P., & Agrawal, T. (2008). *J. Cryst. Growth*, *310*, 2878.
[9] Sharma, B. L. (2003). *Mater. Chem. Phys.*, *78*, 691.
[10] Witusiewicz, V. T., Sturz, L., Hecht, U., & Rex, S. (2004). *Acta Mater.*, *52*, 5071.
[11] Gupta, R. K., Singh, S. K., & Singh, R. A. (2007). *J. Cryst. Growth*, *300*, 415.
[12] Gupta, P., Agrawal, T., Das, S. S., & Singh, N. B. (2012). *J. Chem. Thermodyn.*, *48*, 291.
[13] Agrawal, T., Gupta, P., Das, S. S., Gupta, A., & Singh, N. B. (2010). *J. Chem. Eng. Data*, *55*, 4206.
[14] Das, S. S., Agrawal, T., Gupta, P., & Singh, N. B. (2009). *J. Chem. Eng. Data*, *54*, 1529.
[15] Das, S. S. *et al.* (2009). *Mol. Cryst. Liq. Cryst.*, *501*, 107.
[16] Singh, N. B., Das, S. S., Gupta, P., & Dwivedi, M. K. (2008). *J. Cryst. Growth*, *311*, 118.
[17] Rastogi, R. P., & Verma, K. T. R. (1956). *J. Chem. Soc.*, 2097.
[18] Rastogi, R. P., & Bassi, P. S. (1964). *J. Phys. Chem.*, *68*, 2398.
[19] Callister, W. B. Jr. (2005). *Material Science and Engineering: An Introduction* (6th Ed.), John Wiley & Sons, Inc.: New York, p. 412.
[20] Hillig, H. B., & Turnbull, D. (1956). *J. Chem. Phys.*, *24*, 914.
[21] Wingard, W. C., Majka, S., & Thall, B. M. (1954). *Can. J. Chem.*, *29*, 320.
[22] Singh, N. B., & Dwivedi, K. D. (1982). *J. Sci. Ind. Res.*, *41*, 98.
[23] Rastogi, R. P. (1964). *J. Chem. Edu.*, *41*, 443.
[24] Jackson, K. A. (1958). *Liquid Metals and Solidifications*, ASM: Cleveland, Ohio.
[25] Hunt, J. D., & Jackson, K. A. (1966). *Metall. Soc. AIME*, *236*, 1129.